Supporting Information

Emerging Two-Dimensional Crystallization of Cucurbit[8]uril Complexes: From Supramolecular Polymers to Nanofibers

Jesús del Barrio,[*,†,◊] Ji Liu,[#] Ryan A. Brady,[‡] Cindy S. Y. Tan,[#,○] Stefano Chiodini,[†] Maria Ricci,[‡] Rafael Fernández-Leiro,[⊥] Ching-Ju Tsai,[&] Panagiota Vasileiadi,[¶] Lorenzo Di Michele,[‡] Didier Lairez,[§,♦] Chris Toprakcioglu,[¶] and Oren A. Scherman[*,#]

[†]Instituto de Nanociencia de Aragón, Universidad de Zaragoza, 50018 Zaragoza, Spain. [◊]Departamento de Química Orgánica, Facultad de Ciencias, Instituto de Ciencia de Materiales de Aragón, CSIC–Universidad de Zaragoza, 50018 Zaragoza, Spain. [#]Melville Laboratory for Polymer Synthesis, Department of Chemistry, University of Cambridge, Cambridge CB2 1EW, U.K. [‡]Cavendish Laboratory, Department of Physics, University of Cambridge, JJ Thomson Avenue, Cambridge, CB3 0HE, U.K. [○]Faculty of Applied Sciences, Universiti Teknologi MARA, 94300 Kota Samarahan, Sarawak, Malaysia. [⊥]Spanish National Cancer Research Centre (CNIO), Melchor Fernández Almagro 3, 28029 Madrid, Spain. [&]Laboratory of Biomolecular Research, Division of Biology and Chemistry, Paul Scherrer Institute, Villigen PSI, Switzerland. [¶]Department of Physics, University of Patras, Patras 26500, Greece. [§]Laboratoire Léon Brillouin, CNRS, CEA, Université Paris-Saclay, 91191 Gif-sur-Yvette cedex, France. [♦]Laboratoire des Solides Irradiés, Ecole polytechnique, CNRS, CEA, Université Paris-Saclay, 91128 Palaiseau cedex, France.

E-mail: jdb529@unizar.es (J.D.B), oas23@cam.ac.uk (O.A.S.)

Materials and Methods

Solvents and reagents were obtained from commercial suppliers and used without further purification unless otherwise stated.

IR spectra were recorded using a Perkin-Elmer Spectrum 100 FT-IR spectrometer with an attenuated total reflection (ATR) accessory.

^{1}H NMR and ^{13}C NMR were recorded on a Bruker Avance 500 BB-ATM (500 MHz) spectrometer.

Light scattering experiments were performed on a homemade instrument using an Argon gas laser at wavelength of 515 nm. The light scattered intensity was measured using a Hamamatsu photomultiplier tube connected to a multiple-tau signal correlator from Correlator.com. Measurements were done at different scattering angles using a Newport Micro-Controle goniometer. The light scattering instrument was based on the homodyne technique, or self-beating, with an optical system which was optimized according to previously described procedures (spatial coherence factor was on the order of 0.8).[1]

Small angle X-ray scattering (SAXS) experiments were performed at the SWING beamline of the French synchrotron facility SOLEIL. The X-ray wavelength (λ = 1.24 Å) and sample–detector distance (D = 6375 mm) corresponded to a scattering wavevector range of 0.0015 Å^{-1} < q < 0.15 Å^{-1}. The beam path was held under vacuum conditions, except for a path length of about 1 cm, around the sample. Then scattering data (40 frames of 1 s duration for each sample) were collected with a 17 × 17 cm^2 low-noise AVIEX CCD detector. The 2D scattering images were radially averaged, divided by the transmitted intensity and finally averaged for each sample.

Small angle neutron scattering (SANS) measurements of equimolar mixtures of **2** and CB[8] were performed on the PACE spectrometer at the Laboratoire Léon Brillouin (LLB) neutron facility. D_2O was used as solvent in order to maximize the contrast and minimize incoherent scattering. The samples were placed in quartz cells with a path length of 5 mm, and were measured for 2 h at 25 °C using a neutron wavelength of λ = 1.2 nm and a sample to detector distance of D = 4.6 m. Typical sample transmission was found to be on the order of 0.7. SANS measurements of equimolar mixtures of **3** and CB[8] were performed at the KWS-2 classical pinhole SANS diffractometer of the Heinz Maier-Leibnitz Centre (MLZ) at the FRM II reactor in Garching (München). D_2O was used as solvent in order to maximize the contrast and

minimize incoherent scattering. The samples were placed in quartz cells with a path length of 2 mm. In pinhole geometry, samples were measured at three sample-to-detector distances (D = 1.605, 7.605 and 19.505 m) and 25 °C using a neutron wavelength of λ = 5 or 7 Å (depending on the distance). Typical sample transmission was found to be 0.84–0.87. Data reduction was done following published procedures.[2]

AFM measurements were carried out with an MFP-3D (Classic Oxford Instruments Asylum Research, Santa Barbara, California, USA). The imaging process was performed in amplitude modulation in air and at room temperature using AC240TS cantilevers (Olympus, Tokyo, Japan) with a nominal spring constant of 2 N/m. The set-point to free amplitude ratio was generally kept around to 70% with a free oscillation amplitude of 20 nm. The frequency of excitation was set close to the resonance of the first flexural mode (around 70 KHz). The scan speed was either 1 or 2 Hz obtaining an image of 256x256 pixels with different magnifications. The images were flattened and band-pass filtered using Gwyddion (http://gwyddion.net/) and the data analysis performed with Igor Pro (WaveMetrics, USA). Additional AFM images (for liquid phase and ambient air conditions) were obtained in Tapping Mode using a Multimode 8 AFM microscope equipped with a Nanoscope V control unit from Bruker. All the AFM images were obtained at a scan rate of 0.5–1.2 Hz. For ambient air conditions, RTESPA-150 cantilevers (resonance frequency ≃ 150 kHz, force constant ≃ 6 N/m, nominal values) from Bruker were used. For liquid AFM images SCANASYST-FLUID+ cantilevers from Bruker (resonance frequency in water ≃ 35 kHz, force constant ≃ 0.8 N/m, nominal values) were used.

Isothermal titration experiments were performed on an ITC200 from Microcal Inc. at 298 K in Milli-Q® (Merck Millipore, Feltham, UK) water. The binding constants between CB[8] and guest molecules **2** and **3** were obtained by titrating a solution of a guest molecule (1.0×10^{-3} M) into a cellular CB[8] solution (50.0 μM). Typically 20−50 consecutive injections of ca. 5.0 μL each were used. All solutions were degassed prior to titration. Heats of dilution were determined by titrating an aqueous guest solution into Milli-Q® water. The data was analyzed with Origin 7.0 using a sequential binding model (the first data point was removed from the data set prior to curve fitting as some liquid mixing occurs near the tip of the injection needle at the beginning of each experiment). This analysis is in accordance to previously reported host–guest systems which exhibit analogous binding modes to those of equimolar mixtures of CB[8] and **2** (see Figure S1).[3] Values for the association constants K_a, binding enthalpy ($\Delta H°$), and binding order (stoichiometry) were obtained from the fitted data sets. Standard Gibbs free energy ($\Delta G°$) and entropy changes ($\Delta S°$) were calculated according to equation (Eq. S1).

$$\Delta G° = -RTlnK_a = \Delta H° - T\Delta S° \qquad Eq.S1$$

where *T* is temperature and *R* is the gas constant.

Viscosity measurements were performed using a low shear viscometer LS300 (proRheo GmbH). Steady shear and small-amplitude dynamic shear measurements were performed on a Kinexus pro (Malvern Instruments) and an AR-G2 (TA Instruments) rheometers using a coaxial cylinders geometry, C25 (DIN), with a roughened surface finish. The rheometers were equipped with Peltier-based system for temperature control and a solvent trap to minimize evaporation. Strain sweep measurements were performed at a frequency of 0.1 Hz. The frequency sweep tests were performed within the linear viscoelastic (LVE) regime (determined previously by dynamic strain sweep measurements).

For cryo-EM analysis, samples (3µL) were pipetted onto glow-discharged holey carbon cryo-EM grids (Quantifoil Cu R1.2/1.3), and vitrified in liquid ethane using a Vitrobot (FEI). Data were collected using a Tecnai-F20 electron microscope (FEI) operated at 200kV equipped with a Falcon II direct electron detector (FEI) using a nominal magnification of 50000 x that yielded a calibrated pixel size of 2.08 Å.px^{-1}, a Titan Krios electron microscope (FEI) operated at 300 kV and equipped with a K2 Summit direct electron detector (Gatan) mounted after a Gatan Imaging Filter (GIF) using a 20eV slit to remove inelastic scattered electrons using a nominal magnification of 105000x that yielded a calibrated pixel size of 1.19 Å.px^{-1}, or a Talos Arctica microscope (FEI) operated at 200 kV and equipped with Falcon III direct electron detector at a nominal magnification of 120000x (calibrated pixel size of 0.89 Å.px). Images were collected using a total dose of 40 e/Å^2 as a single frame on the Falcon II detector, as 20 frame image stacks on the K2 detector using a flux of 2 e/Å^2/sec and electron counting mode, and as 32 frame image stacks on the Falcon III detector using a flux of 1 e$^-$/Å^2/frame in electron counting mode. Frames were aligned and averaged using MOTIONCOR2.[4] Contrast transfer function parameters were calculated using Gctf.[5] All subsequent data processing was done using the software packages Focus and MRC Image Processing Programs.[6]

The lyotropic properties of the fibers were investigated using a customized Zeiss HAL100 microscope. Samples of CB[8]·**3** (1:1 ratio, in water) at about 0.2 wt. % were concentrated up to a concentration of ca. 1.0 wt. % prior to use.

X-ray diffraction (XRD) data was obtained in a PANalytical Empyrean X-ray diffractometer equipped with a PIXcel^{1D} detector using Cu-Kα radiation (λ = 1.5418 Å). Samples of CB[8]+**3** and CB[8]+**2** (1:1 ratio, in water) at about 0.2 wt. % were concentrated up to a concentration of ca. 2.5 wt. % prior to use.

The fluorescence measurements were obtained in a PerkinElmer LS 55 luminescence spectrometer. Both incubated and fresh samples of CB[8]+**3**, 1:1 ratio (1.0×10^{-3} M, in milli-Q® water), were prepared as discussed below (page S7) and diluted with milli-Q® water (ca. 0.8×10^{-3} mM, final concentration) prior to use.

Synthesis and Characterization of CB[7], CB[8] and Guest Molecules 2 and 3

All starting materials were purchased from Sigma-Aldrich and used as received unless stated otherwise. Guest molecule 1-methyl-3-[(naphthalen-2-yl)methyl)-imidazolium bromide (**1**), 1,3-bis[(naphthalen-2-yl)methyl]-imidazolium bromide (**2**), CB[7] and CB[8] were synthesized according to previously described methods.[7–9] Guest molecule **3** was prepared from the reaction of 1-[(naphthalen-2-yl)methyl]-1*H*-imidazole[8] and *α*,*α*'-dibromo-*p*-xylene as shown in Scheme S1.

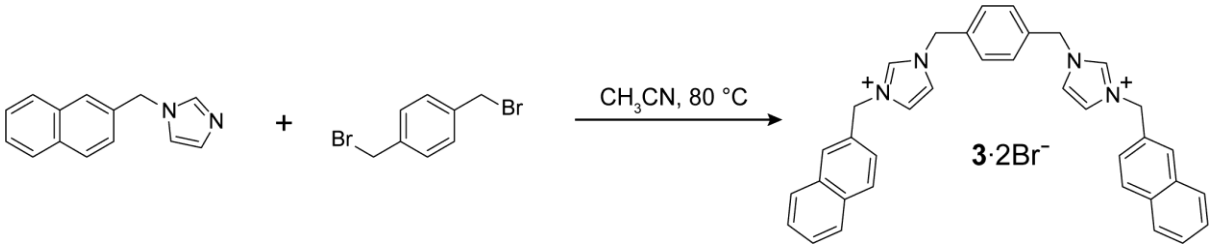

Scheme S1. Synthesis of guest molecule **3**.

***α*,*α*'-Bis{3-[1-(naphthalen-2-yl)methyl]-imidazolium}-*p*-xylene dibromide (3)**

α,*α*'-Dibromo-*p*-xylene (0.26 g, 1.0 mmol) and 1-[(naphthalen-2-yl)methyl]-1*H*-imidazole[8] (0.48 g, 2.3 mol) were dissolved in hot acetonitrile (ca. 30 mL). The mixture was stirred and heated at 80 °C for 96 h. During this time, a white solid precipitated from the solution. The flask was cooled down to room temperature and the precipitate was isolated from the reaction mixture by filtration. The filter cake was washed with acetonitrile and diethyl ether and dried under reduced pressure. The crude product was recrystallized twice from a mixture of acetonitrile and ethanol (0.25 g, 37%). M.p. 172–175 °C (dec.). FTIR (neat) ν (cm^{-1}): 3162, 3076, 2961, 2835, 1598, 1560, 1512, 1188, 1174, 1152. ^{1}H NMR (500 MHz, DMSO-d_6) δ (ppm): 9.50 (s, 2H), 8.02–7.87 (m, 10H), 7.85 (s, 2H), 7.62–7.51 (m, 6H), 7.49 (s, 4H), 5.61 (s, 4H), 5.45 (s, 4H). ^{13}C NMR (125 MHz, DMSO-d_6) δ (ppm): 135.34, 132.74, 132.69, 132.06, 129.00, 128.98, 128.83, 127.87, 127.72, 127.70, 126.83, 126.79, 125.75, 123.08, 122.85, 52.27, 51.57. LRFABMS *m/z* $[M - 2Br]^{2+}$ calcd for $C_{36}H_{32}N_4$: 260, found: 260. Anal. calcd. for $C_{36}H_{32}Br_2N_4$: C, 63.54; H, 4.74; N, 8.23; found: C, 63.58; H, 4.76; N, 8.21.

Preparation of Inclusion Complex Solutions

The preparation procedure of CB[8] complexes of **2** and **3** is as follows. The required amount of guest molecules **2** and **3** was first weighted and then dissolved separately in Milli-Q® water, or a solution of sodium chloride (Figure S11), to produce 0.02–0.20 wt. % stock solutions. An aliquot (ca. 20 mL) of an individual guest molecule stock solution was transferred to a vial containing the appropriate amount of CB[8]. Such mixture was stirred and sonicated simultaneously at 293 K for 2 min. Pulsed sonication was applied with a Hielscher Ultrasonic Processor UP200Ht at 35 W equipped with a titanium sonotrode. The diameter of the sonotrode was 0.7 cm. The amplitude value was 50%. A pulse-duty cycle of 10% was selected (the maximum power transmitted to the sample in each pulse was ca. 68 W/cm^2). Samples prepared in this way were allowed to equilibrate under static conditions at 293 K for a minimum period of ca. 24 h unless otherwise stated.

Isothermal Titration Calorimetry Studies

The binding of guest **2** to CB[8] was analyzed in an analogous fashion to previously reported positively-charged small molecule systems exhibiting two naphthalene moieties.[3] The sigmoidal shape of the curve facilitates the estimation of the midpoint of the transition, and thus the absolute stoichiometry of the binding reaction between CB[8] and the naphthalene moieties of **2**; in this case 2:1 (Figure S1a). This means that two naphthalene moieties bind simultaneously to CB[8] and therefore, the absolute binding ratio of **2** to CB[8] is 1:1. Complexation thermodynamics for the binding equilibrium between guest **2** and CB[8] was analyzed using a sequential binding model: $K_{a,1}$ = (7.0 ± 0.3) × 10^4 M^{-1}; $\Delta H_1°$ = -7.6 ± 0.3 kcal/mol; $\Delta G_1{}^o$ = -6.6 ± 0.1 kcal/mol; $T{\cdot}\Delta S_1{}^o$ = -1.0 ± 0.2 kcal/mol; $K_{a,2}$ = (1.2 ± 0.3) × 10^6 M^{-1}, $\Delta H_2°$ = -15.7 ± 0.1 kcal/mol; $\Delta G_2{}^o$ = -8.3 ± 0.2 kcal/mol, $T{\cdot}\Delta S_2{}^o$ = -7.4 ± 0.3 kcal/mol. Since $K_{a,2} >> K_{a,1}$ and the complementary species CB[8] and **2** are always mixed at an equimolar ratio, linear polymer formation can occur in the mM concentration range. This is evident from our morphological analysis (*vide infra*). The binding of guest molecule **3** to CB[8] was analyzed in an analogous fashion to that of guest molecule **2** (*vide supra*). When a solution of guest molecule **3** was added dropwise into a solution of CB[8], a transition is observed at a molar ratio of ca. 1 (Figure S1b). This suggests that two molecules of CB[8] can simultaneously bind to **3** at the beginning of the titration experiment; when the host is in excess with respect to the guest. With continued addition of guest into the host solution, a second transition occurs; which evidences the formation of a host–guest complex with either 1:1 or *n*:*n* (supramolecular polymer) stoichiometry.

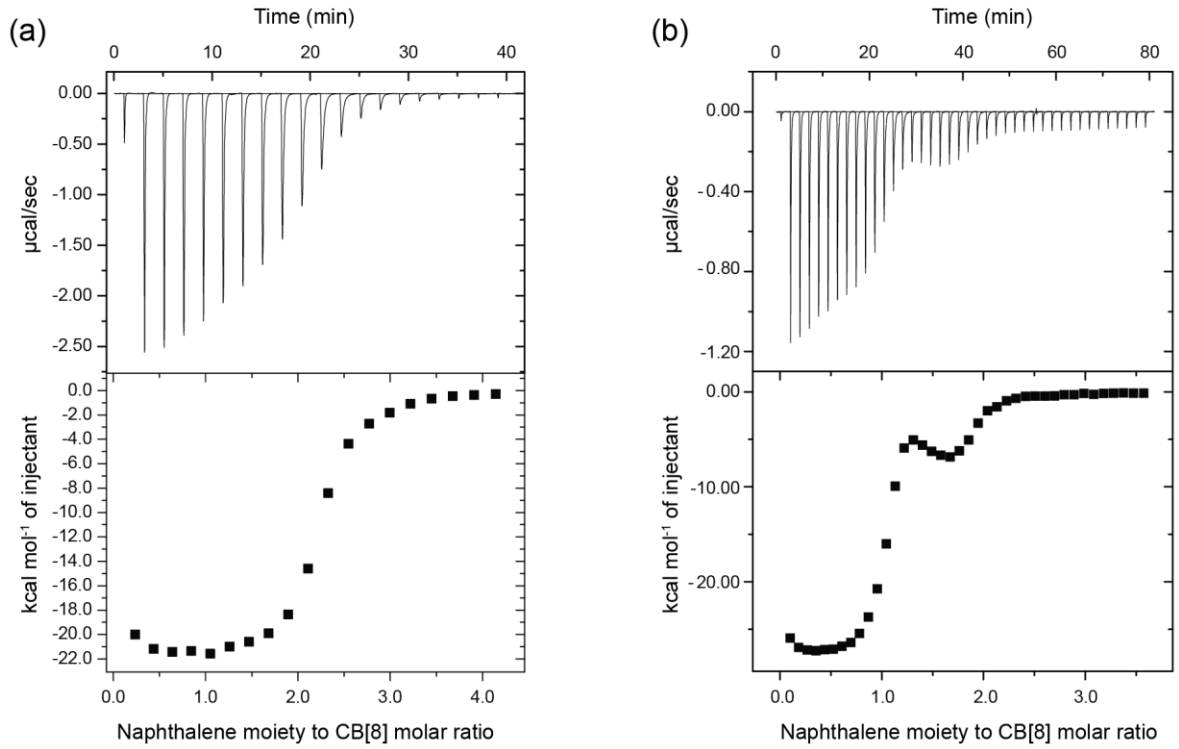

Figure S1. Representative ITC experiments of **2** (a) and **3** (b) binding to CB[8].

Small Angle X-ray Scattering Measurements

The SAXS pattern of an incubated sample of CB[8] and **2** (equimolar, 1.0 mM) in heavy water is shown in Figures S2 and S3. A scattering pattern characteristic of a Gaussian chain structure with a radius of gyration (R_g) of ca. 31 nm was obtained from our SAXS measurements on equimolar (1.0 mM) mixtures of CB[8] and **2** in water (Figure S2). The semiflexible nature of the polymer chains was also supported by SANS measurements (Figure S8). The scattering intensity $I(q)$ in Figure S2 was fitted to the Debye scattering function for Gaussian chains.[10]

$$I(q) = \frac{2(e^{-x} + x - 1)}{x^2} \qquad Eq.S2$$

where $x = < R_g^2 \, q^2 >$, with the radius of gyration treated as a fitting parameter. In the high q region (0.008 Å < q < 0.1 Å), the most significant scatterers are the semiflexible chains of CB[8]$_n$·**2**$_n$. However, these species only have a minor contribution to the scattering in the low q region, where the scattering associated with the large platelet-like structures is dominant (Figures S3 and S4). This is related to the q^{-1} power-law behavior in the low q region, as shown by static light scattering (Figures S4).

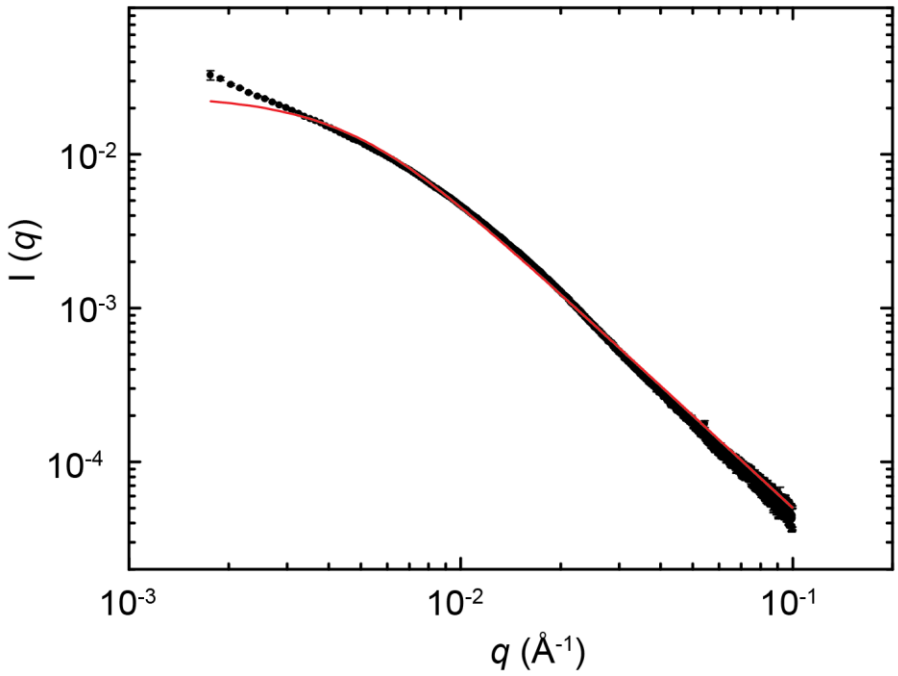

Figure S2. SAXS pattern of an equimolar (1.0 ×10^{-3} M) mixture of CB[8] and **2** in D_2O after incubation. The continuous curve is a least squares fit to the Gaussian chain model with a mean R_g of 31 nm. At high values of q (i.e. $q \times R_g >> 1$) the Debye scattering function scales with q^{-2}.

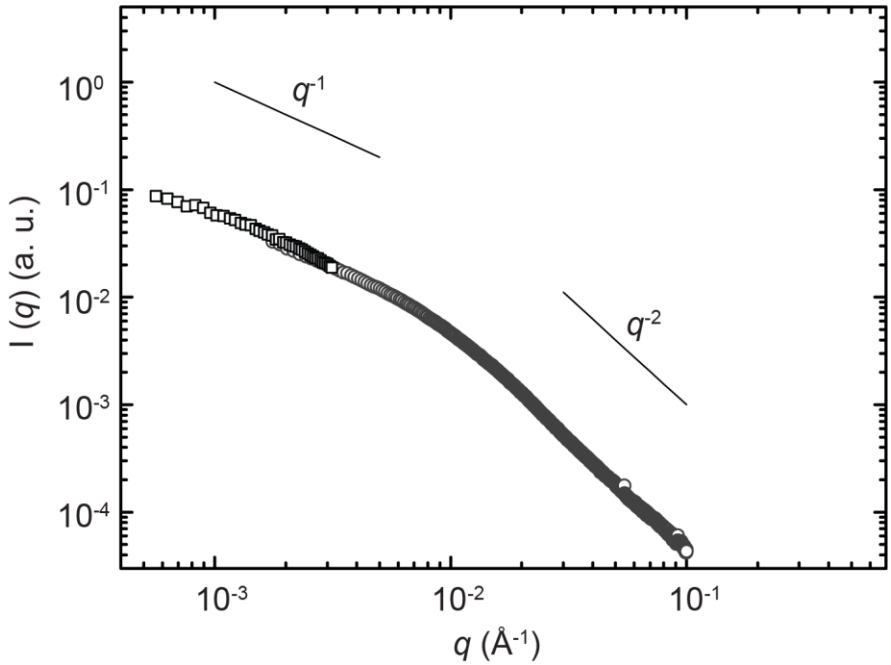

Figure S3. Combined SAXS (circles) and SLS (squares) measurements for an equimolar (1.0 mM) mixture of CB[8] and **2** in D_2O after incubation. The scattering intensity of the SLS data (*vide infra*) has been rescaled to the scattering intensity of the SAXS data in the 0.002 Å < q < 0.003 Å region.

Static Light Scattering Measurements

The SLS pattern of an incubated sample of CB[8] and **2** (equimolar, 1.0 Mm) in heavy water is shown in Figures S3 and S4.

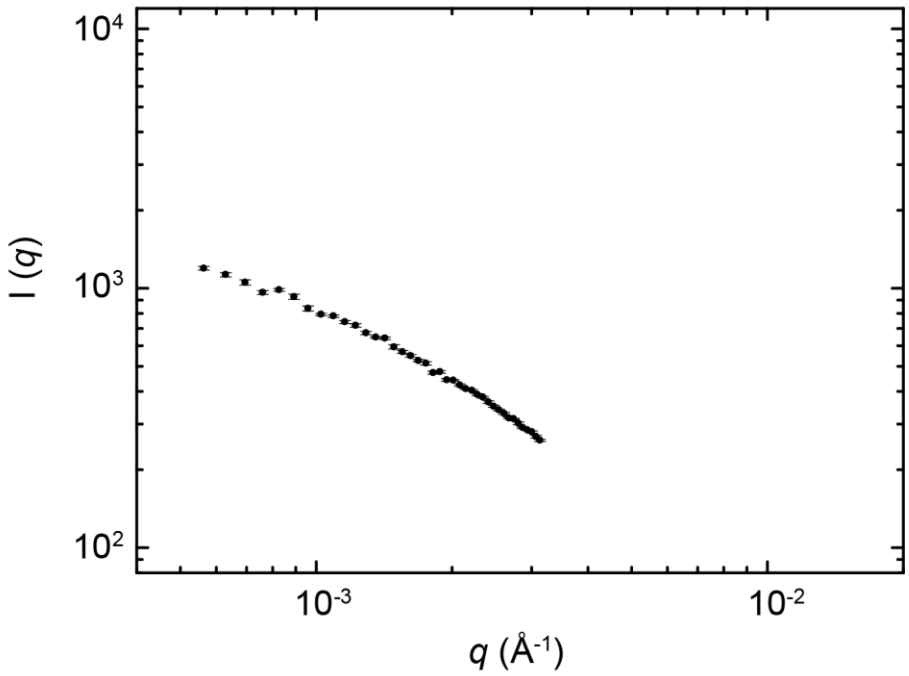

Figure S4. SLS pattern of an equimolar (1.0×10^{-3} M) mixture of CB[8] and **2** in D_2O after incubation.

The dynamic structure factor $S(q, t)$, was extracted from the correlation function, $g(t)$, of the scattered light intensity. The dynamic structure factor was then fitted with a stretched exponential:

$$S(q,t) = exp\left[-\left(\frac{t}{\tau}\right)^{\beta}\right] \qquad Eq.S3$$

With two fitting parameters, β and τ. A β value of 0.82 ± 0.03 and an apparent diffusion coefficient (D) of ca. 7×10^{-8} $cm^2\ s^{-1}$ were obtained. A value of hydrodynamic radius (R_h) of ca. 30 nm was obtained by using the Stokes–Einstein relationship

$$D = \frac{k_B T}{6\pi\eta R_h} \qquad Eq.S4$$

where k_B is the Boltzmann constant, η is viscosity and T is temperature.

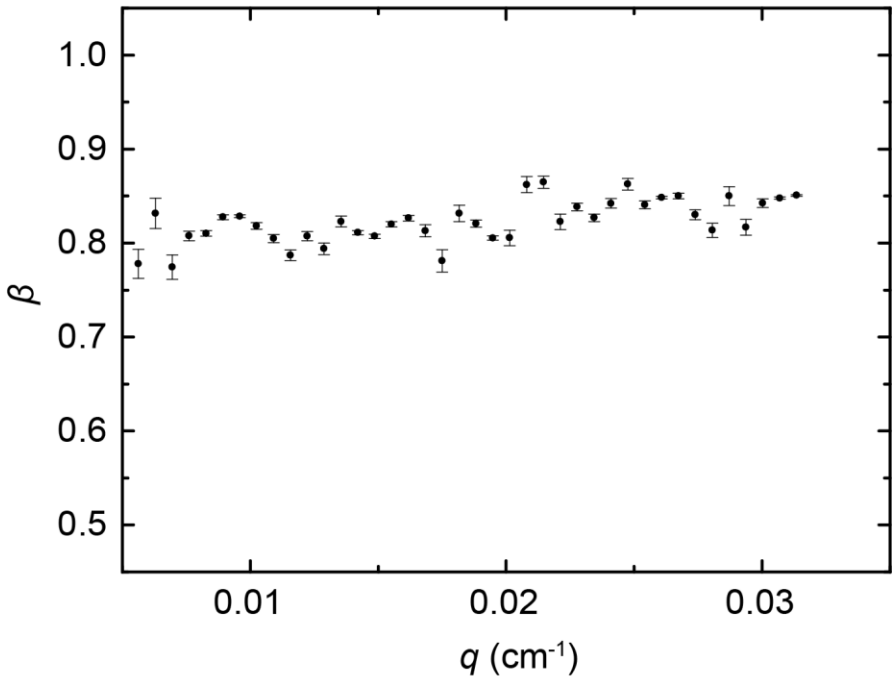

Figure S5. Dependence of the stretching parameter, β, as a function of the scattering vector magnitude, q. A value of 0.82 ± 0.03 is apparent from the data.

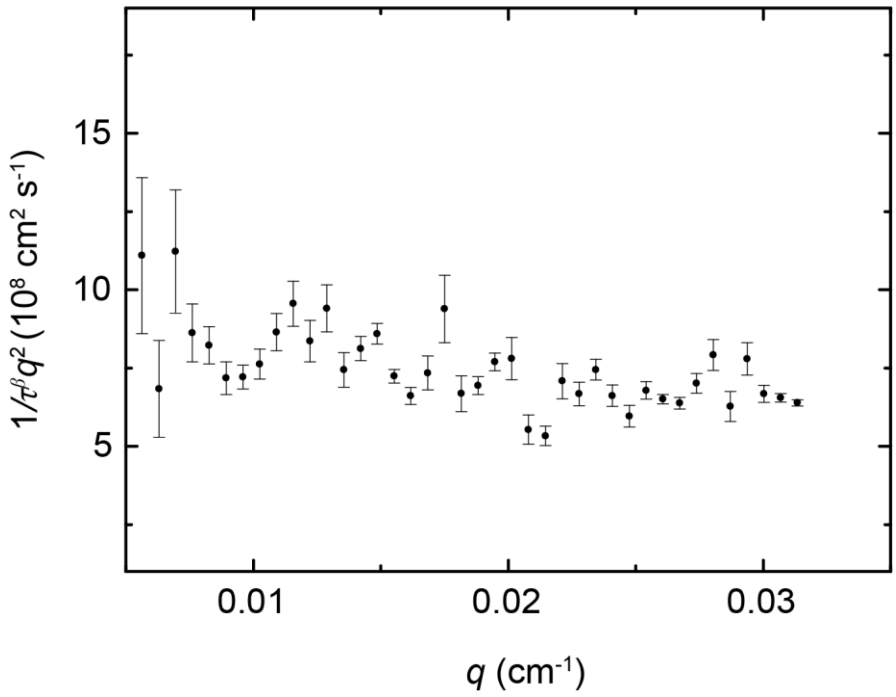

Figure S6. Apparent diffusion coefficient as a function of the scattering vector magnitude, q.

Small Angle Neutron Scattering Measurements

The SANS pattern of incubated sample of CB[8] + **3** and CB[8] + **2** in heavy water are shown in Figures S7 and S8. For CB[8] + **3** there is a clear power-law dependence of q^{-2} in the high-q region (0.006 Å < q < 0.03 Å), which is attributed to the presence of semiflexible polymer chains of CB[8]$_n$·**3**$_n$. The additional scattering at low q values (0.003 Å < q < 0.006 Å) follows a q^{-1} power law, which is a signature of elongated structures. These results parallel those obtained for CB[8] + **2** by SAXS and SLS (Figure S3). For CB[8] + **2**, only the high-q region was investigated by SANS (Figure S8).

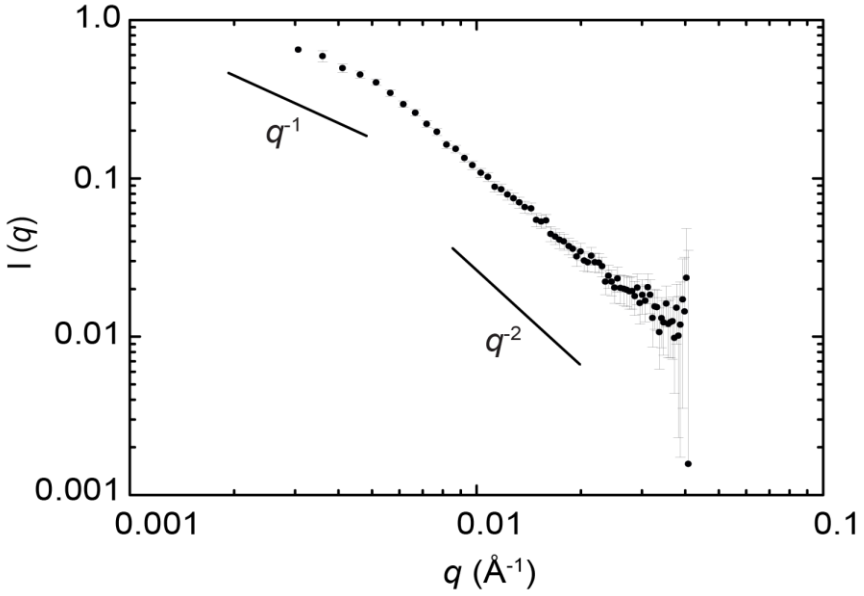

Figure S7. SANS pattern of an equimolar (1.0×10^{-3} M) mixture of CB[8] and **3** in D_2O.

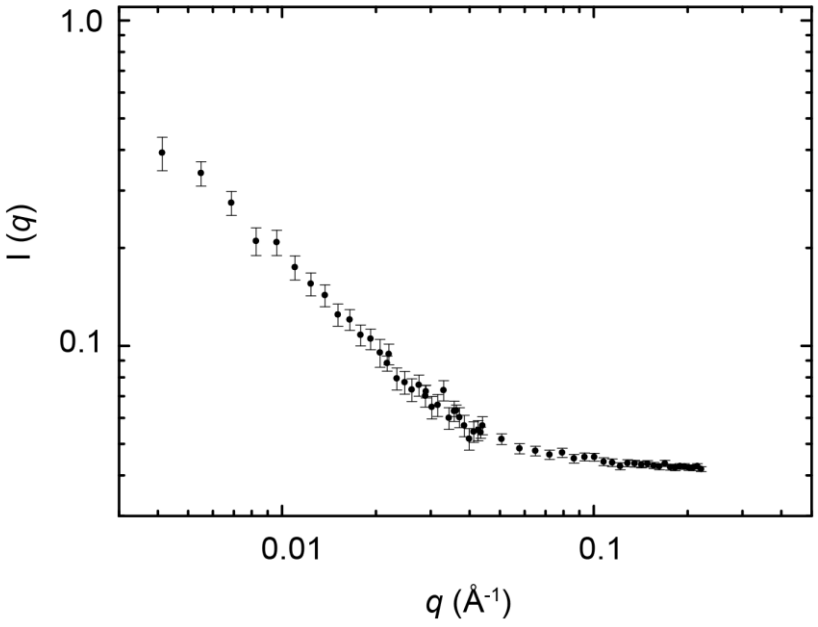

Figure S8. SANS pattern of an equimolar (1.0×10^{-3} M) mixture of CB[8] and **2** in D_2O.

Atomic Force Microscopy Studies

Preliminary morphological AFM images were obtained from samples of the CB[8] complexes of guest molecules **2** and **3** were incubated at 293 K for a period of ca. 24 h unless otherwise stated. Samples were diluted with milli-Q® water (5–10 times) immediately before performing analysis with AFM. Approximately 20 µL of the diluted samples were deposited on freshly cleaved mica disks. Samples casted in this way were allowed to stand at room temperature for 2 min. Then, most of the solution was removed by carefully approaching a piece of filter paper to the edge of the mica disks. Mica disks (9.9 mm of diameter, Agar Scientific, Stansted, Essex, UK) were glued on microscope slides (76x26 mm, 1.0–1.2 mm thickness, ground edges, 45° clear glass, Academy Science Product, Beckenham, UK) with epoxy glue (Araldite rapid, Araldite Professional Adhesives, Basel, Switzerland). The samples were placed on the AFM sample stage and fixed with magnetic holders.

Additional liquid AFM morphological analysis was performed on samples of the CB[8] complexes of guest molecules **2** and **3**. Approximately 50 µL of the samples were deposited on freshly cleaved mica disks. Before beginning the measurement, the cantilever-sample system was allowed to reach the thermal equilibrium for a minimum of 30 min. The height statistical analysis and individual height profiles were carried out using Gwyddion (http://gwyddion.net/). All the images were flattened with a plane and a 2nd order polynomial subtraction. Additionally, a median of differences rows alignment was applied. The average widths were corrected from the AFM convolution artefact as reported in literature.[11] The width and length of the CB[8]$_n$·**2**$_n$ platelet-like aggregates was obtained by considering a minimum of 20 different line profiles and found to be ca. 35±9 nm and 121±55 nm respectively. The average height of the platelet-like aggregates was between 2.1 and 4.2 nm (in those cases that the mica surface was partially covered with unaggregated CB[8]$_n$·**2**$_n$ the height of the aggregates was determined at the intersection of two platelet-like aggregates). The average length of the CB[8]$_n$·**3**$_n$ fibers was impossible to determine because typical lengths are larger than the scan size used in the experiment (maximum scan size was 15 µm). The analysis of the height distribution of the CB[8]$_n$·**3**$_n$ fibers by liquid AFM is shown in Figure S10c. The width of the CB[8]$_n$·**3**$_n$ fibers was obtained by considering a minimum of 20 different line profiles and found to be ca. 41±16 nm (somewhat wider fibers are obtained after incubation periods of more than 24 hours)

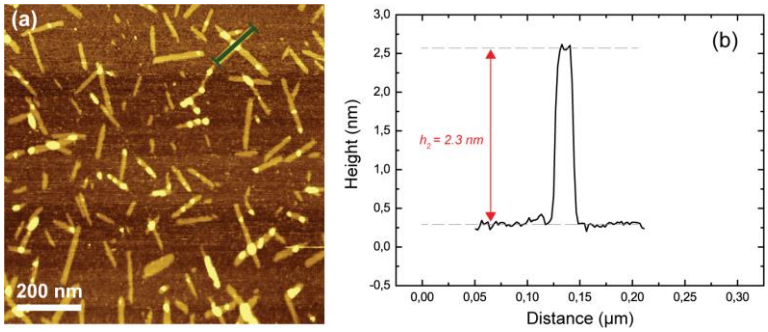

Figure S9. Liquid AFM morphological analysis of the CB[8]$_n$·**2**$_n$ platelet-like aggregates (a), and a representative AFM line profile (b), shown in (a) as a green line.

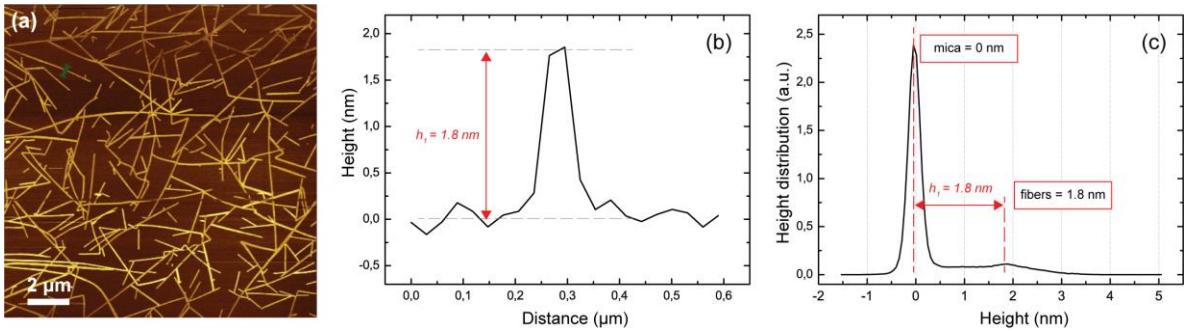

Figure S10. Liquid AFM morphological analysis of a sample of the CB[8]$_n$·**3**$_n$ fibers (a), a representative AFM line profile (b), shown in (a) as a green line. The histogram corresponding to the height (thickness) analysis of the fibers is shown in (c). The distance between the maxima of the two populations of values in (c) is associated with the thickness of the fibers.

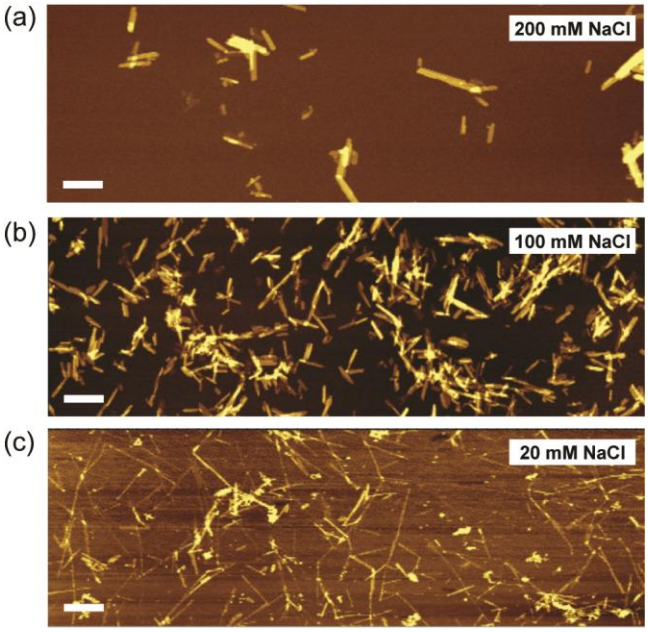

Figure S11. AFM morphological analysis of aqueous mixtures of CB[8] + **3** (1.0×10^{-3} M) in the presence of NaCl. Size of the white bar is 1 μm in all images.

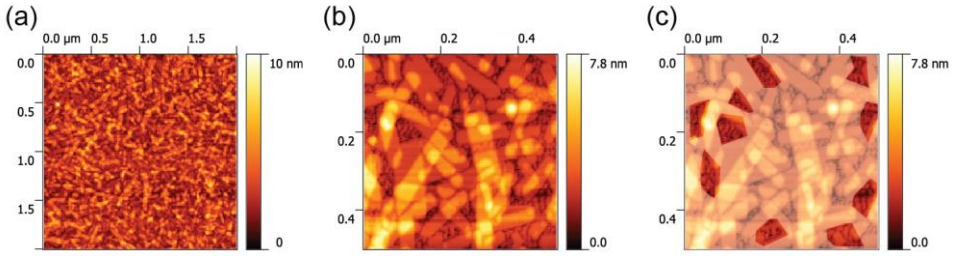

Figure S12. AFM morphological analysis of incubated samples of CB[8]$_n$·**2**$_n$. Images (b) and (c) are the same except that highlighted areas in (c) contain globular aggregates of semiflexible chains of CB[8]$_n$·**2**$_n$ predominantly.

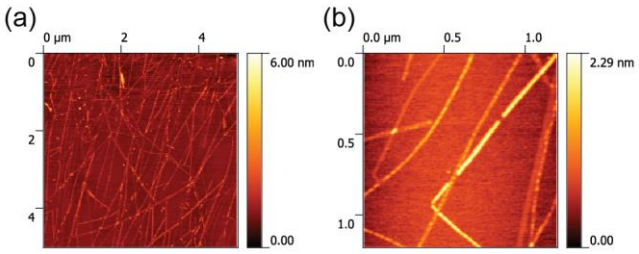

Figure S13. AFM morphological analysis of incubated samples of CB[8]$_n$·**3**$_n$.

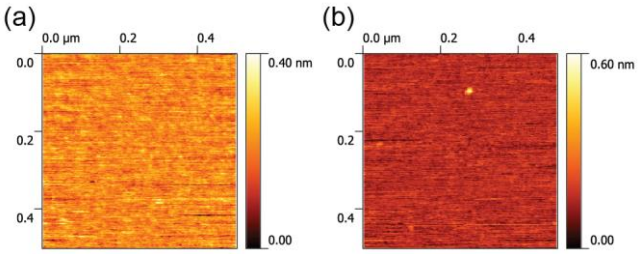

Figure S14. AFM morphological analysis of incubated aqueous samples (milli-Q® water, 1.0×10^{-3} M) of **2** (a) and **3** (b).

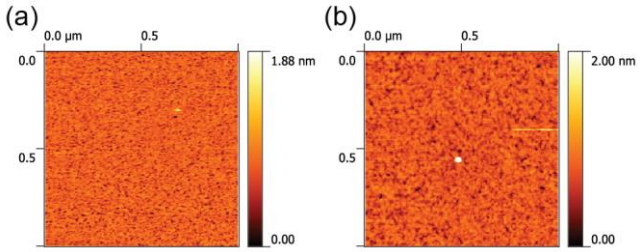

Figure S15. AFM morphological analysis of freshly prepared (incubation time was limited to ca. 2 min) equimolar (milli-Q® water, 1.0×10^{-3} M) mixtures of CB[8] + **2** (a) and CB[8] + **3** (b).

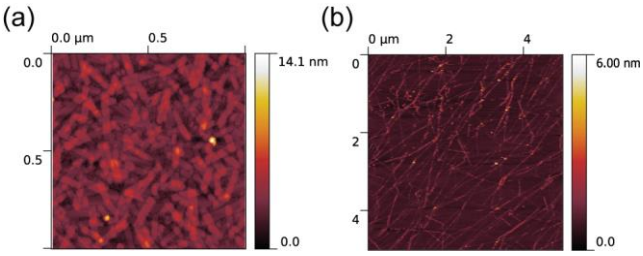

Figure S16. AFM morphological analysis of incubated (24 hours) equimolar (3.0×10^{-3} M) mixtures of CB[8] and **2** (a), and CB[8] and **3** (b).

High-resolution Cryo-electron Microscopy Studies

A high-resolution cryo-EM micrograph of an individual fiber is shown in Figure S17. After a preliminary selection, 21 images were continued for data processing, from which 29 crystal lattices were unbent twice to correct the lattice distortions. Initial symmetry assignment was calculated using ALLSPACE, suggesting $P22_12_1$ as the highest symmetry. During merging, unsuitable lattices were rejected due to their high phase residuals. At the end, 11 lattices were merged together, giving a projection resolution of ~3.9 Å.

Table S1. Electron crystallographic images statistics

Plane group symmetry	$p22_12_1$
Unit cell parameters	
a (Å)	22.6 ± 0.3
b (Å)	36.4 ± 0.4
γ (°)	90
Processed images	21
Processed lattices	29
Number of lattices used for merging	11
No. of observed reflections to 3 Å	1061
No. of unique reflections to 3 Å	72
Phase residual (°)	
Resolution shell	
200 – 9.5 Å	5.5
9.5 – 6.7 Å	14.9
6.7 – 5.5 Å	3.0
5.5 – 4.7 Å	3.7
4.7 – 4.2 Å	9.6
4.2 – 3.9 Å	10.1
3.9 – 3.6 Å	40.7
3.6 – 3.4 Å	42.6
3.4 – 3.2 Å	48.8
3.2 – 3.0 Å	30.3
Overall to 3.0 Å	22.5

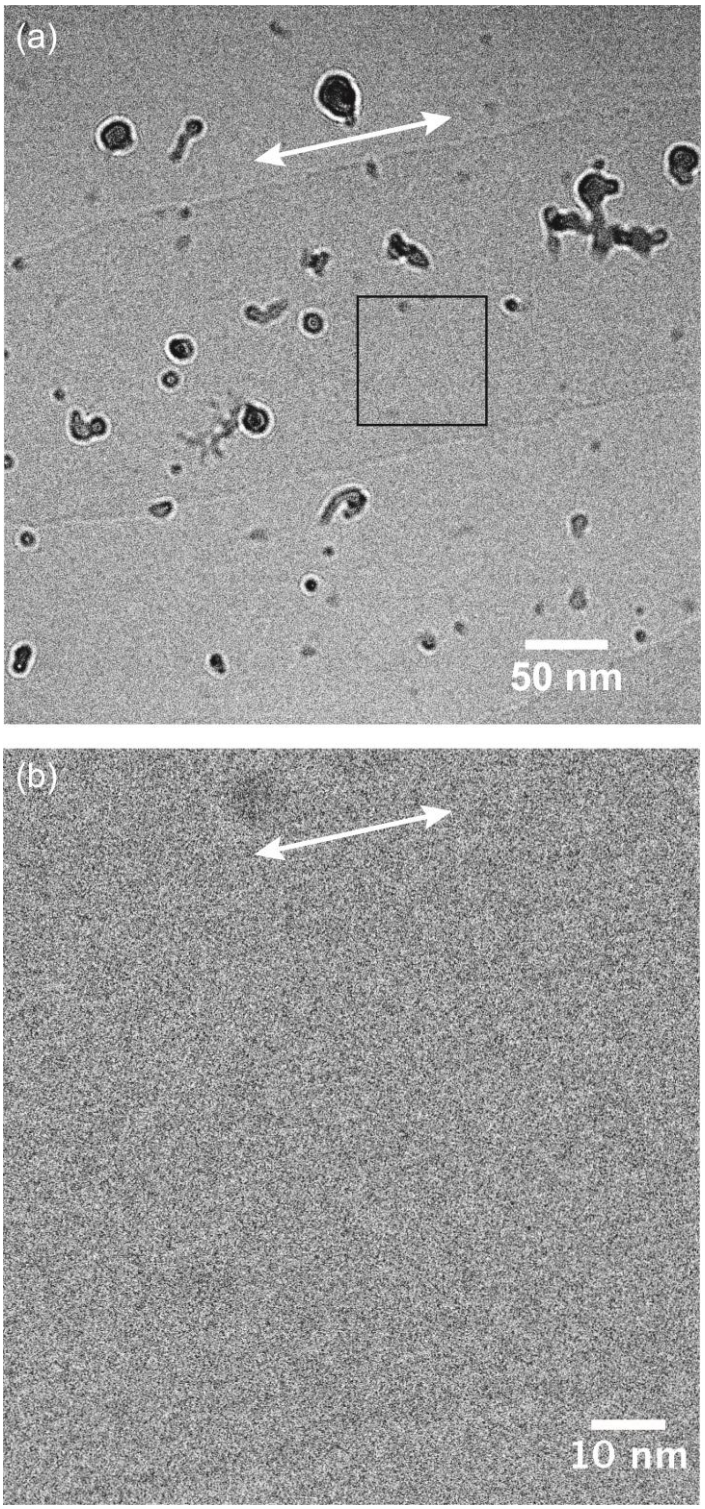

Figure S17. High-resolution cryo-EM micrograph of an individual fiber of CB[8]$_n$·**3**$_n$ (a). Magnified area showing a lamellar microstructure of alternating light and dark domains possibly associated to the polymer chains of CB[8]$_n$·**3**$_n$ (b). Double arrow (a, b) indicates the fiber long axis. Note that high-contrast blobs in (a) are artefacts associated with contamination from cryo-EM sample preparation.[12]

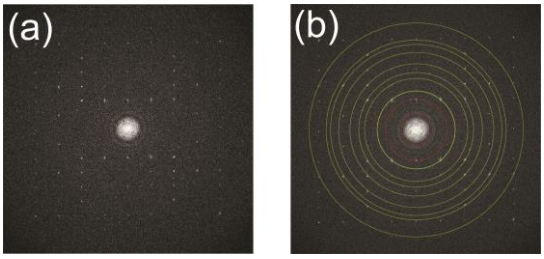

Figure S18. FFT of the magnified image in Figure S17. Circles in (b) highlight diffraction peaks present in the XRD pattern of Figure 3.

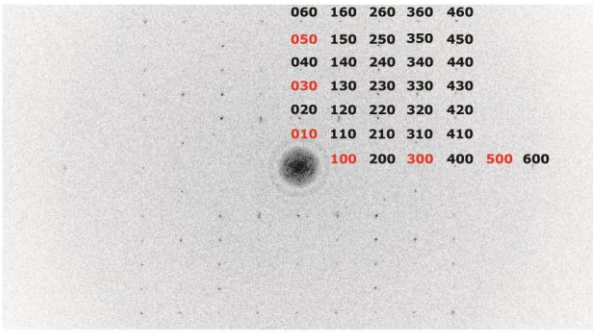

Figure S19. Indexed FFT pattern assuming a $P2_12_12$ unit cell. Red labels indicate systematic absences

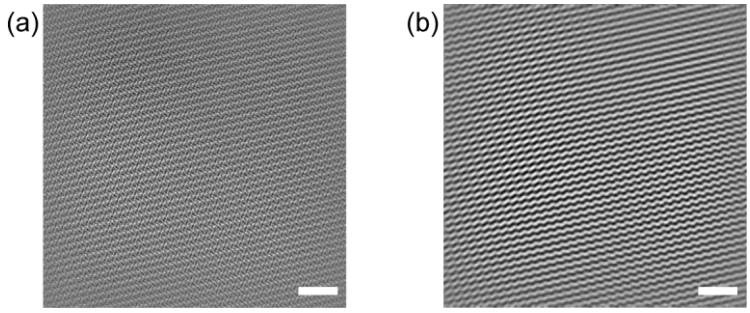

Figure S20. The inverse FFT reconstruction from the masked FFT pattern in Figure S18 before (a) and after (b) lowpass filtering the image to 12.5 Å. Size of white bar is 10 nm.

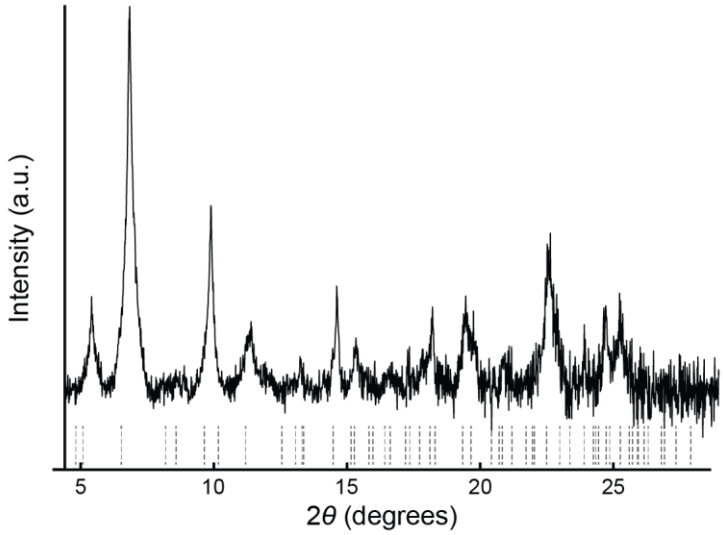

Figure S21. XRD pattern corresponding to an incubated mixture (equimolar) of CB[8] and **3** in water. Dashed vertical lines indicate the best fits of the pattern to the predicted Bragg peaks {hkℓ} planes with ℓ = 0, assuming $P2_12_12$.

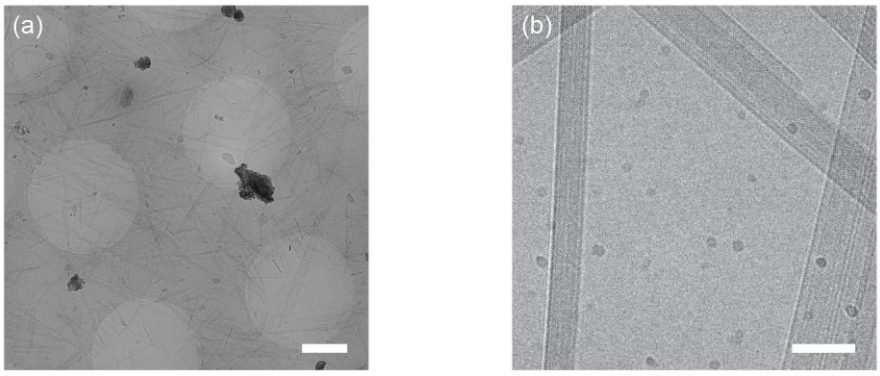

Figure S22. High-resolution cryo-EM micrograph of a sample of platelet-like aggregates of CB[8]$_n$·**2**$_n$ (a) and magnified area showing the microstructure of the aggregates (b). Size of white bar is 500 nm (a) and 50 nm (b). The aspect ratio of the platelet-like aggregates imaged by cryo-EM is somewhat higher than that found by AFM measurement (*vide supra*), which could be associated with a partial break-up of the aggregates during sample preparation, *prior* to AFM imaging. Note that high-contrast blobs in Figure S22a are artefacts associated with contamination from cryo-EM sample preparation (ethane contamination during freezing of the sample and/or plastic contamination from grid-support-layer manufacturing).[12]

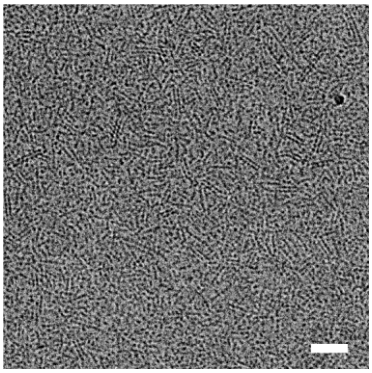

Figure S23. TEM morphological analysis of an equimolar (milli Q® water, 1.0×10^{-3} M) mixtures of CB[8] + **2** after a short incubation of ca. 2 min. Size of white bar is 50 nm.

Rheological Measurements

Incubated samples of CB[8]$_n$·**3**$_n$ exhibit a viscoelastic behavior reminiscent of the Maxwell model (Figure 4). However, the data do not fit a single-element Maxwell model. Instead, the fitting was performed according with a multi-element Maxwell model:

$$G'(\omega) = \sum_k G_k \frac{\omega^2 \tau_k^2}{1 + \omega^2 \tau_k^2} \qquad Eq.S5$$

$$G''(\omega) = \sum_k G_k \frac{\omega \tau_k}{1 + \omega^2 \tau_k^2} \qquad Eq.S6$$

where G' and G'' are the storage and loss moduli, respectively; G_k and τ_k are the G_0 and τ_r for the k^{th} element, respectively; ω is the oscillation frequency.[13] As there is an obvious deviation from the pure Maxwell behavior, the multi-element fitting provides a more quantitative interpretation of the small-amplitude dynamic shear measurements. The number of elements chosen was exclusively based on the minimal number required to obtain a reasonably good fit and they have no attributable physical meaning. The solid lines in Figure S25 show the fits obtained for a 3-element Maxwell model and the values of the parameters obtained are listed in Table S2. The plateau modulus G_0 is the sum of the three moduli G_1–G_3 (Table S2) according to:

$$G_0 = \sum_k G_k \qquad Eq.S7$$

For simplicity, only G_0 values and the longest relaxation time of each set of τ_{r1}–τ_{r3} values (Table S2) are discussed in this study.

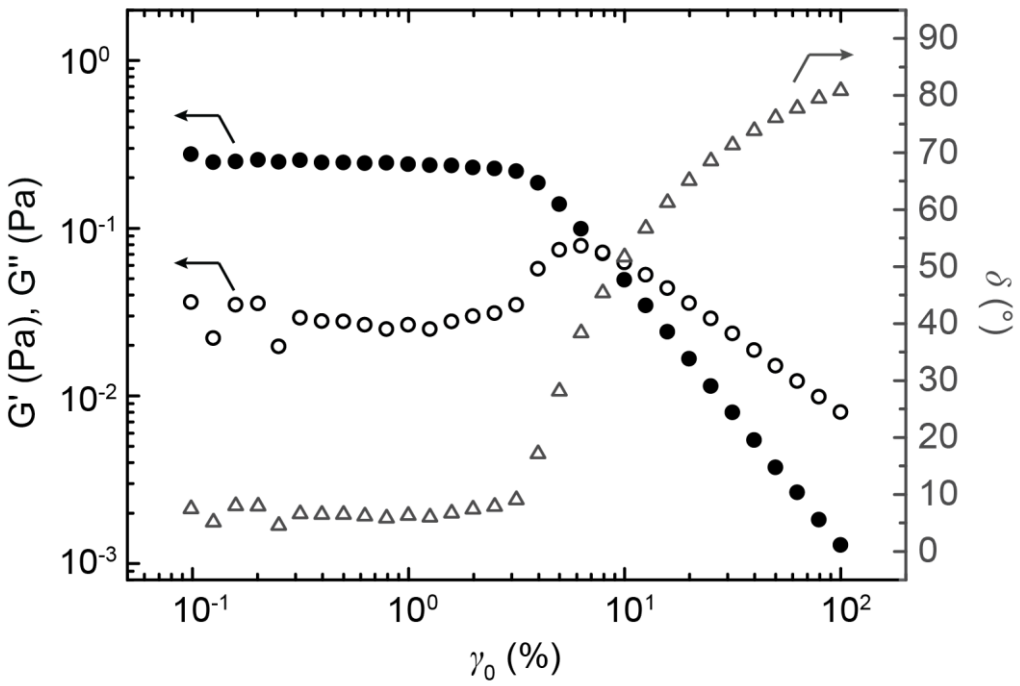

Figure S24. Representative storage modulus (closed symbols) and loss modulus (open symbols) dependence on amplitude from a dynamic oscillatory test at 293 K and 0.1 Hz corresponding to an incubated mixture of CB[8] (1.0×10^{-3} M) and **3** (1.0×10^{-3} M) in water.

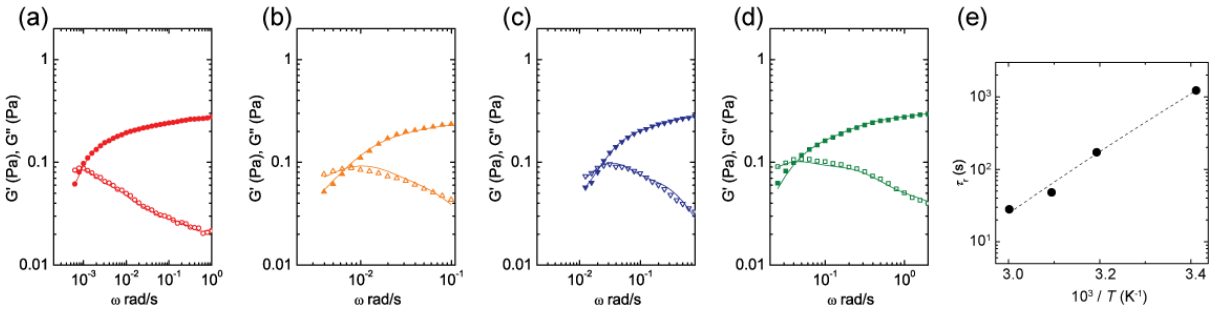

Figure S25. Storage modulus (closed symbols) and loss modulus (open symbols) dependence on frequency corresponding to an incubated mixture of CB[8] (1.0×10^{-3} M) and **3** (1.0×10^{-3} M) in water at 293 (a), 313 (b), 323 (c) and 333 K (d); and Arrhenius plot of the relaxation time, τ_r, versus 10^3/T (e). Continuous lines in (a–d) are fits to the Maxwell model with 3 elements.

Table S2. Summary of the rheological parameters extracted from the frequency sweep measurements (see Figure S25).

	T = 293K	T = 313K	T = 323K	T = 333K
G_1 (Pa)	0.0464	0.0490	0.0505	0.0518
G_2 (Pa)	0.0637	0.0930	0.1001	0.1083
G_3 (Pa)	0.1540	0.1513	0.1599	0.1660
G_0 (Pa)	0.2641	0.2933	0.3105	0.3261
τ_{r1} (s)	12.20	1.561	0.897	0.470
τ_{r2} (s)	135.4	29.78	5.834	4.200
τ_{r3} (s)	1226	172.3	47.55	27.90

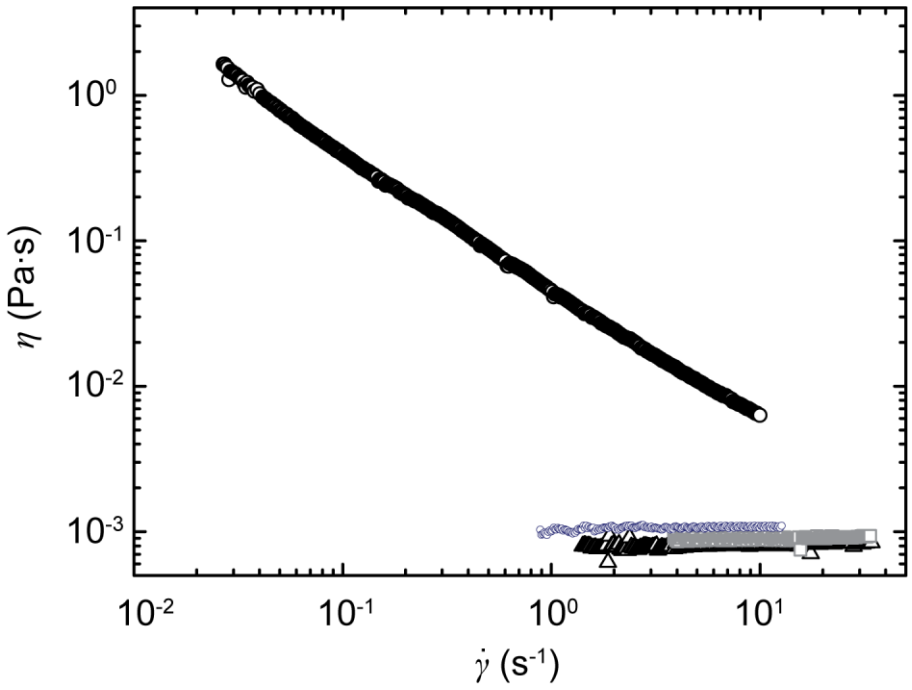

Figure S26. Shear viscosity as a function of shear rate for an aqueous solution of **3** (1.0×10^{-3} M) alone after incubation (open grey squares), an equimolar (1.0×10^{-3} M) mixture of CB[8] and **3** before (open black triangles) and after (open black circles) incubation, and an equimolar (1.0×10^{-3} M) mixture of CB[8] and **2** after 24 hours of incubation (open blue circles).

Rheological Measurements --- Kinetics of Fiber Formation

The preparation procedure of CB[8] complexes of **3** for kinetic studies is as follows. The required amount of **3** was first weighted and then dissolved separately in Milli-Q® water to produce a stock solution. An aliquot (ca. 20 mL) of a stock solution of **3** was transferred to a vial containing the appropriate amount of CB[8]. Such mixture was stirred and sonicated simultaneously at 293 K for 2 min, and immediately transferred to the measuring cell of the rheometer. Kinetic information can be obtained by following the temporal evolution of properties including the elastic modulus (G'), loss modulus (G'') and complex viscosity (η^*). We have analyzed the temporal evolution of η^* of CB[8]$_n$·**3**$_n$ according to previously reported procedures.[14] Analogous trends have been obtained from the temporal evolution of G', instead of η^*. The growth of fibrous networks and gels has been analyzed in the past according to the Avrami theory,[15] which describes the nucleation and growth of bulk crystal processes as follows:

$$ln[1 - X_{cr}] = -kt^n \qquad Eq.S8$$

where k is a temperature-dependent parameter (analogous to a rate constant), t is time and X_{cr} is equal to $\varphi(t)/\varphi(\infty)$, where $\varphi(t)$ is the volume fraction of the crystal material at t, and $\varphi(\infty)$ is $\varphi(t)$ at $t \rightarrow \infty$. The Avrami exponent n is temperature independent; and its theoretical value (1–4, as well as half integers) is determined by the nature of the nucleation and crystal growth. For one-dimensional (rod-like), two-dimensional (plate-like) and three-dimensional (spherical) growth; n = 1, 2, and 3 respectively. In fractal growth, the length of the bulk crystals in previous considerations should be replaced by the radius of gyration and n by the fractal dimension D_f. Therefore, for fractal growth, Eq. S8 can be expressed as:

$$ln[1 - X_{cr}(t)] = -k(t - t_g)^{D_f} \qquad Eq.S9$$

Liu and co-workers have introduced Eq. S10 to describe the growth of a 3D network associated to a gelling system,[14] where gelation takes place after t_g. In such model, $X_{cr}(t)$ is given by:

$$X_{cr}(t) = \frac{\eta^*(t) - \eta_0}{\eta^*(\infty) - \eta_0} \qquad Eq.S10$$

where η_0 is the viscosity of the solvent, $\eta^*(t)$ is the complex viscosity of the system at t and $\eta^*(\infty)$ is $\eta^*(t)$ at $t \rightarrow \infty$. In Figures 4b and S27, the temporal evolution of η^* of CB[8]$_n$·**3**$_n$ fibers is represented. At very early times, η^*, G' and G'' are very low. After an induction period, both G' and G'' increase and then plateau. The final G' value is much larger than that of G'', which indicates the formation of a viscoelastic system. In Figure S27b, a plot of ln{–ln[1–$X_{cr}(t)$]} values versus ln(t–t_g) for t_1–t_2 period yields a relatively good linear fit; which means that the geometrical properties are independent of the size increase of the gyration of the fiber system during the growth. From these quantitative analysis, a $D_f \sim 1$ is obtained, which is consistent with the morphological analysis. An analogous treatment of the temporal evolution of G' gives values of D_f that are very close to 1. The mechanical perturbations associated with rheological measurements may influence the kinetics of fiber growth. Inadequate experimental parameters could, in principle, induce fibril break-up and; therefore, significantly alter the system. Nevertheless, it is reasonable to propose that the aggregation patterns and associated D_f values (*vide supra*) would remain unaffected. To minimize any potential perturbation associated with the rheological measurements, all kinetic experiments were performed at 0.3% strain (well within the LVE) and at 0.1 s^{-1}. An accepted mechanism for the growth of many molecular gelators and fibrous systems includes stochastic nucleation followed by the growth of the nucleated species.[16] An analogous particle formation process may be assumed for CB[8]$_n$·**3**$_n$ fibers. A large variation of induction times (50–300 min) was observed for the formation of the fibers, which may be related to the random nature of the initial nucleation step.[15]

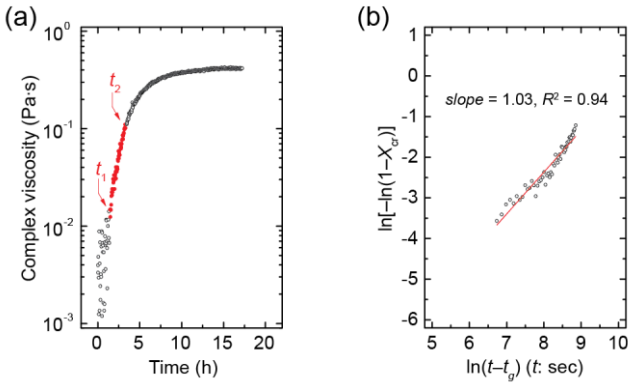

Figure S27. Dependence of η^* as a function of time (a) for an aqueous equimolar mixture of **3** and CB[8] (1.0×10^{-3} M, H_2O, 293 K) and corresponding Avrami plot (b).

Packing Model

The packing model was build using the software CrystalMaker®.[17] The 5 Å resolution cryo-EM maps show the location of the CB[8] molecules with the encapsulated naphthalene groups of **3**. A previous structure of a CB[8] homoternary complex based on a naphthalene-containing guest molecule was employed for the initial configurations of the naphthalene groups of **3** bound to CB[8].[18] Fragments of the guest molecule **3** were built and relaxed using ChemBio3D Ultra 13.0. Such fragments were then combined with the initial configuration of the CB[8] molecules with the encapsulated naphthalene groups of **3** to approximately match the 4 Å resolution cryo-EM maps yielding the structure of CB[8]$_n$·**3**$_n$. A final relaxation of the hydrogen atoms was performed with CrystalMaker®.[17] Other geometrical calculations and molecular graphics were performed using PyMOL and MERCURY.[19]

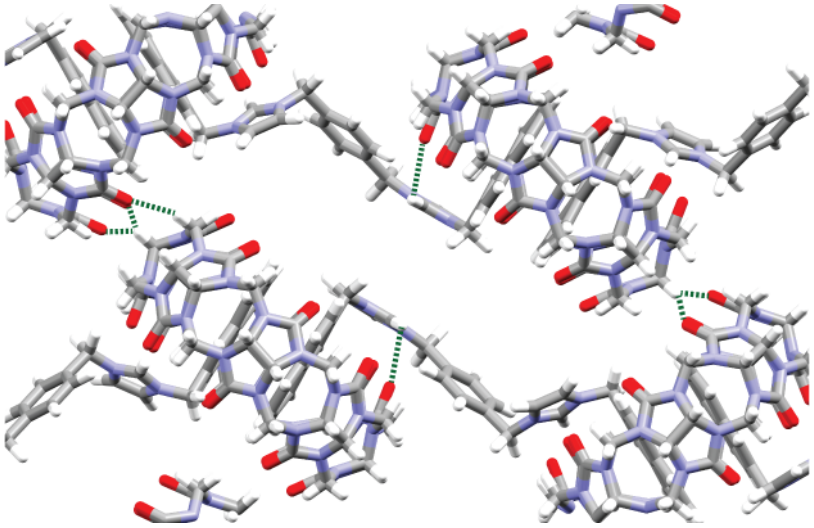

Figure S28. Packing model showing hydrogen bonding interactions between **3** and CB[8] and between molecules of CB[8] themselves (green dotted lines).

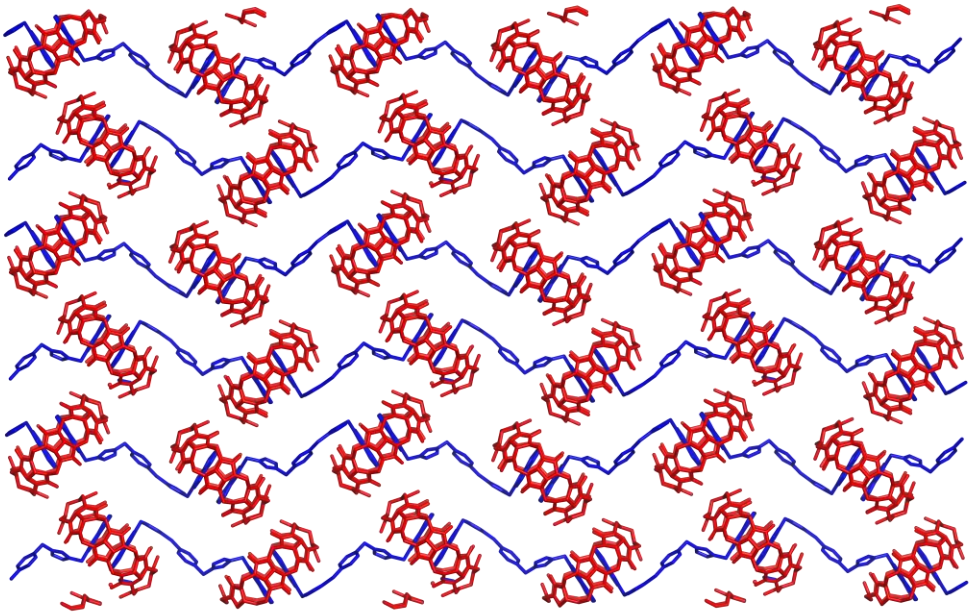

Figure S29. Packing model (3x3) of CB[8]$_n$·**3**$_n$ showing the CB[8] molecules (in red) and **3** (in blue).

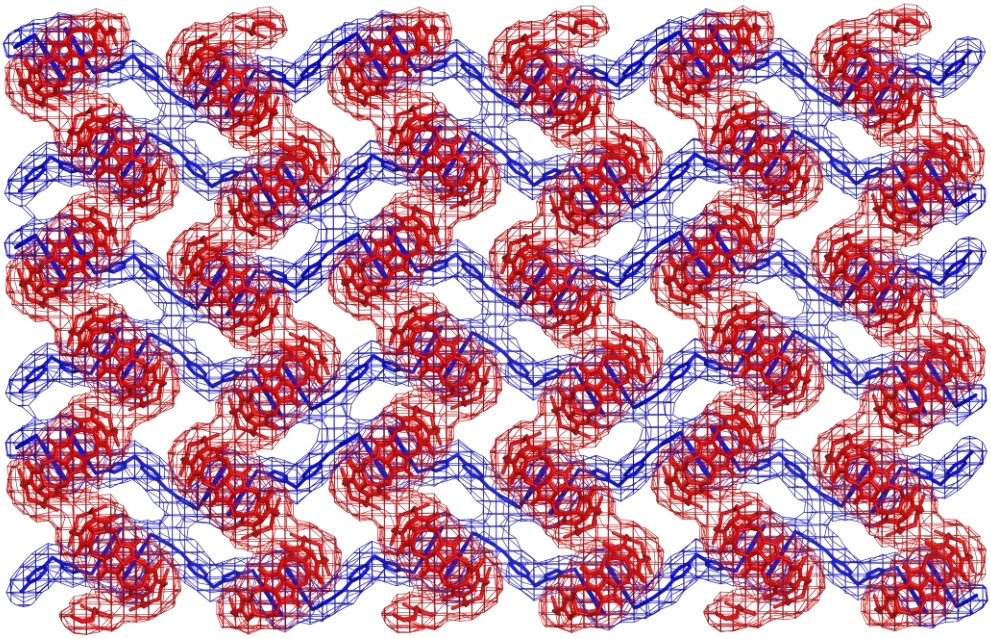

Figure S30. Packing model (3x3) of CB[8]$_n$·**3**$_n$ and van der Waals surface map.

Fluorescence Measurements

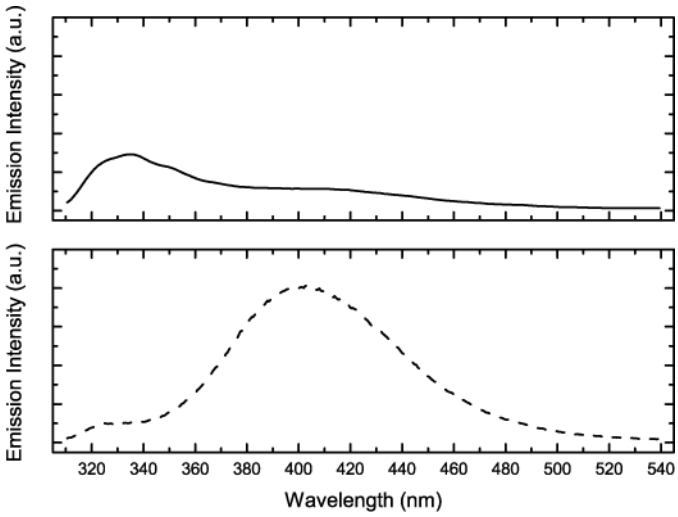

Figure S31. Fluorescence spectra (λ_{exc} = 290 nm) of a fresh (solid line) and an incubated sample (dashed line) of CB[8] + **3**.

References

1. Chu, B. Laser Light Scattering; Academic Press: Boston, 1991.

2. Brulet, A.; Lairez, D.; Lapp, A.; Cotton, J.-P. *J. Appl. Cryst.* **2007**, *40*, 165–177.

3. (a) Kang, Y.; Cai, Z.; Huang, Z.; Tang, X.; Xu, J.-F.; Zhang, X. *ACS. Macro Lett.* **2016**, *5*, 1397–1401. (b) Liu, Y.; Liu, K.; Wang, Z.; Zhang, X. *Chem. Eur. J.* **2011**, *17*, 9930–9935.

4. Zheng, S. Q.; Palovcak, E.; Armache, J.-P.; Verba, K. A.; Cheng, Y.; Agard, D. A. *Nat. Methods* **2017**, *14*, 331–332.

5. Zhang, K. *J. Struct. Biol.* **2016**, *139*, 1–12.

6. (a) Biyani, N.; Righetto, R. D.; McLeod, R.; Caujolle-Bert, D.; Castano-Diez, D.; Goldie, K. N.; Stahlberg, H. *J. Struct. Biol.* **2017**, *198*, 124–133. (b) Crowther R. A.; Henderson. R.; Smith, J. M. *J. Struct. Biol.* **1996**, *116*, 9–16.

7. Jiao, D.; Biedermann, F.; Tian, F.; Scherman, O. A. *J. Am. Chem. Soc.* **2010**, *132*, 15734–15743.

8. Wright, B. D.; Deblock, M. C.; Wagers, P. O.; Duah, E.; Robishaw, N. K.; Shelton, K. L.; Southerland, M. R.; DeBord, M. A.; Kersten, K. M.; McDonald, L. J.; Stiel, J. A.; Panzner, M. J.; Tessier, C. A.; Paruchuri, S.; Youngs. W. J. *Med. Chem. Res.* **2015**, *24*, 2838–2861.

9. Kim, J.; Jung, I. S.; Kim, S. Y.; Lee, E.; Kang, J. K.; Sakamoto, S.; Yamaguchi, K.; Kim, K. *J. Am. Chem. Soc.* **2000**, *122*, 540–541.

10. Debye, P. *J. Phys. Colloid. Chem.* **1947**, *51*, 18–32.

11. Canet-Ferrer, J.; Coronado, E.; Forment-Caliaga, A.; Pinilla-Cienfuegos, E. *Nanotechnology*, **2014**, *25*, 395703.

12. Grassucci, R. A.; Taylor, D. J.; Frank, J. *Nat. Protoc.* **2007**, *2*, 3239–3246.

13. Afifi, H.; da Silva, M. A.; Nouvel, C.; Six, J.-L.; Ligoure, C.; Dreiss, C. A. *Soft Matter* **2011**, *7*, 4888–4899.

14. Liu, X. Y.; Sawant, P. D. *Adv. Mater.* **2002**, *14*, 421–426.

15. Estroff, L. A.; Hamilton, A. D. *Chem. Rev.* **2004**, *104*, 1201–1218.

16. Weiss, R. G.; Terech, P. *Molecular Gels: Materials with Self-Assembled Fibrillar Networks;* Springer: Dordrecht, 2006.

17. Palmer, D. C. (2014). CrystalMaker. CrystalMaker Software Ltd, Begbroke, Oxfordshire, England.

18. Gao, Z-Z.; Lin, R-L.; Bai, D.; Tao, Z.; Liu, J-X.; Xiao, X., *Sci. Rep.* **2017**, *7*, 44717.

19. Macrae, C. F.; Bruno, I. J.; Chisholm, J. A.; Edgington, P. R.; McCabe, P.; Pidcock, E.; Rodriguez-Monge, L.; Taylor, R.; van de Streek, J.; Wood, P. A. *J Appl Crystallogr.* **2008**, *41*, 466–470.